Computational discovery of stable M_{2}AX phases

Michael Ashton, Richard G. Hennig, Scott R. Broderick, Krishna Rajan, and Susan B. Sinnott

Computational Discovery of Stable M$_2$AX Phases

Michael Ashton and Richard G. Hennig
Department of Materials Science and Engineering,
University of Florida, Gainesville, FL 32611-6400

Scott R. Broderick and Krishna Rajan
Department of Materials Design and Innovation,
University at Buffalo, The State University of New York, Buffalo, NY 14260

Susan B. Sinnott
Department of Materials Science and Engineering,
The Pennsylvania State University, University Park, PA 16801-7003
(Dated: August 15, 2016)

The family of layered M$_{n+1}$AX$_n$ compounds provides a large class of materials with applications ranging from magnets, to high-temperature coatings, to nuclear cladding. In this work, we employ a density-functional theory based discovery approach to identify a large number of thermodynamically stable M$_{n+1}$AX$_n$ compounds, where $n = 1$, M = Sc, Ti, V, Cr, Zr, Nb, Mo, Hf, Ta; A = Al, Si, P, S, Ga, Ge, As, Cd, In, Sn, Tl, Pb; and X = C, N. We calculate the formation energy for 216 pure M$_2$AX compounds and 10,314 solid solutions, $(MM')_2(AA')(XX')$, relative to their competing phases. We find that the 49 experimentally known M$_2$AX phases exhibit formation energies less than 30 meV/atom. Among the 10,530 compositions considered, 3,140 exhibit formation energies below 30 meV/atom, most of which have yet to be experimentally synthesized. A significant subset of 301 compositions exhibits strong exothermic stability in excess of 100 meV/atom, indicating favorable synthesis conditions. We identify empirical design rules for stable M$_2$AX compounds. Among the metastable M$_2$AX compounds are two Cr-based compounds with ferromagnetic ordering and expected Curie temperatures around 75K. These results can serve as a map for the experimental design and synthesis of previously unknown M$_2$AX compounds.

Keywords: materials discovery, MAX Phase, stability, magnetic nanolaminates

I. INTRODUCTION

The synergistic relationship between computational and experimental methods has redefined materials discovery and design. The accuracy of density-functional methods in predicting ground state properties of compounds, coupled with the increasing capabilities of modern supercomputer infrastructures, enables the computational prediction and design of compounds to meet new technological needs. The vision that state-of-the-art computational methods allow the screening of vast compositional spaces for selected properties in a matter of days to weeks is becoming a reality, and can aid experimental efforts. For example, compositions spanning nearly the entire periodic table have been screened for stability and piezoelectric-related properties,[1,2] over 2000 compounds have been systematically investigated for their properties as Li-intercalation electrodes,[3] and the thermal conductivities of 75 compounds were predicted computationally and discovered to correlate linearly with their experimental values.[4] In each case, the interpretation of results and design of screening parameters has drawn heavily on experimental knowledge.

The hexagonal layered ceramic compounds known as MAX phases represent one such vast composition space, and one that has proven to be a fertile frontier for materials discovery over the last five decades.[5] The flexible M$_{n+1}$AX$_n$ formula (M = Sc, Ti, V, Cr, Zr, Nb, Mo,
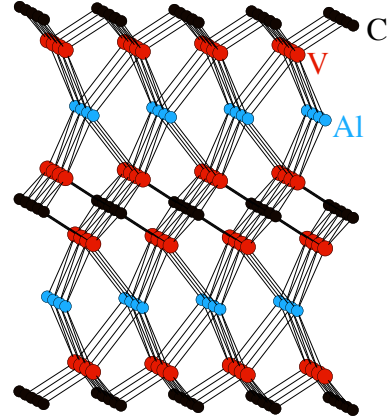

FIG. 1. Crystal structure of V$_2$AlC, a representative member of the M$_2$AX phase family.

Hf, Ta; A = Al, Si, P, S, Ga, Ge, As, Cd, In, Sn, Tl, Pb; X = C, N; n = 1, 2, 3) is responsible for the large size of the MAX phase family. Over 60 compositions have been synthesized already,[6] including solid solution mixtures of M, A, and/or X species.[7–13] All MAX phases share the same crystal structure, shown in Figure 1 for V$_2$AlC as an example. The recently reported synthesis of MAX phases with new compo-

sitions suggests that the compositional space of MAX phases has not yet been exhausted.[14,15] The list of potential applications for MAX phases is quite long, and includes magnets,[16] high-temperature protective coatings,[17] low-friction coatings,[18,19] heating elements,[20] electrical contacts,[21] radiation cladding,[22,23] and impact-absorption materials,[9] among others. They can even be chemically etched to produce two-dimensional transition metal carbides and nitrides,[24–26] which have shown aptitude for application in ionic battery anodes.[27–29]

Considerable work has already been performed to establish the stability of members in the MAX phase family,[30–33] but never in the solid solution compositional space, and the selection of competing phases was generally performed in an *ad hoc* manner. The solid solution space is particularly interesting, as solid solutions often provide improved mechanical properties over their end members[9,34,35] and in some cases are stable even when neither end member is.[36]

The ability to accurately determine phase stability from first-principles calculations hinges largely on our ability to identify the most stable competing phases for each composition. Hand-selecting these phases without error from experimental phase diagrams requires meticulous and time-consuming analysis that is only feasible for a small number of compounds at a time. Screening a large compositional space requires a consistent, systematic approach that lends itself to, and even requires, computation. Here, we extend the use of modern high-throughput screening techniques and first-principles calculations to screen the entire $n = 1$ $M_{n+1}AX_n$ phase family (hereafter referred to as M_2AX phases) for thermodynamic stability. The $n = 1$ stoichiometry is chosen because it represents the simplest and smallest unit cell, and includes 49 out of the 61 experimentally synthesized MAX phases, thus allowing our predictions to be readily compared to experimental results. Our strategy can be extended to screen the $n = 2$ and $n = 3$ $M_{n+1}AX_n$ stoichiometries in future work.

In this study we apply a high-throughput framework coupled to density-functional theory calculation for phase stability, described in Sec. II, to screen the large number of possible M_2AX phases for previously unknown compounds. We show in Sec. III B that all 49 experimentally synthesized M_2AX phases have low formation energies of less than 30 meV/atom relative to competing phases. Among the 10,530 compositions considered, we identify 3,140 with formation energies below 30 meV/atom and 301 with strong exothermic stability in excess of 100 meV/atom. We identify trends and design rules in Sec. III D and determine that two Cr-based M_2AX show ferromagnetic ordering with magnetic moments above 1 μ_B. Our predictions provide guidance to experimental efforts for the synthesis of previously unknown M_2AX compounds.

II. COMPUTATIONAL APPROACH

To achieve computational tractability, we limit our search to consider only 50-50 solid solutions for all three of the M, A, and X components. Lower resolution stoichiometries would require larger periodic cells. Interestingly, all but one, $(Ti_{0.75}Nb_{0.25})_2AlC$,[7] of the experimentally synthesized solid solution MAX phases are close to 50-50 ratios for the M, A and/or X components. In the case of $(Ti_{0.75}Nb_{0.25})_2AlC$, a corresponding $(Ti_{0.55}Nb_{0.45})_2AlC$ MAX phase was also synthesized, indicating that considering only 50-50 solid solutions will still identify most or all compositional systems in which stability is possible. Therefore, a resolution of 0.5/formula unit is chosen for all three of the M, A and X sites in the present work. Applying this constraint aids the investigation in two ways: it narrows the number of compositions to 10,530, and enables the use of periodic cells containing only 8 atoms (4 M, 2 A, and 2 X). Figure 2 illustrates the six unique atomic configurations for these 8 atom cells.

To complete the non-trivial task of selecting the most thermodynamically stable competing phases for these 10,530 compositions, we systematically survey the Materials Project database,[37] containing structural and thermodynamic data obtained by density-functional calculations for more than 58,000 compounds. The use of this database for thermodynamic screening in similar high-throughput searches has been demonstrated to result in occasional overestimates of thermodynamic stability but only rarely in underestimates.[2]

To determine the stability of the M_2AX compounds, we perform density-functional theory (DFT) calculations for the M_2AX compounds and all competing phases using the VASP package,[38,39] a plane-wave code using the projector-augmented wave method.[40,41] We select the Perdew-Burke-Ernzerhof (PBE) generalized-gradient approximation to the exchange-correlation functional,[42] which has been widely used in high-throughput DFT calculations[1,2,43] and shown to accurately reproduce structures and formation energies for solid systems.[44–48] A plane-wave cutoff energy of 520 eV and a k-point mesh with a density of 500 k-points per atom ensure energy convergence to within 5 meV/atom and cell volumes to within 2.5% for over 70% of compounds in a high-throughput test.[43] These input settings are based on the default parameters used by the Materials Project structural database.[49,50] The Brillouin-zone integration is performed with the Methfessel-Paxton scheme as implemented in VASP with a smearing of 0.1 eV. To detect magnetic M_2AX phases, we include spin-polarization in all calculations. The M_2AX compounds and all competing phases are relaxed until the energy changes by less than 10^{-4} eV.
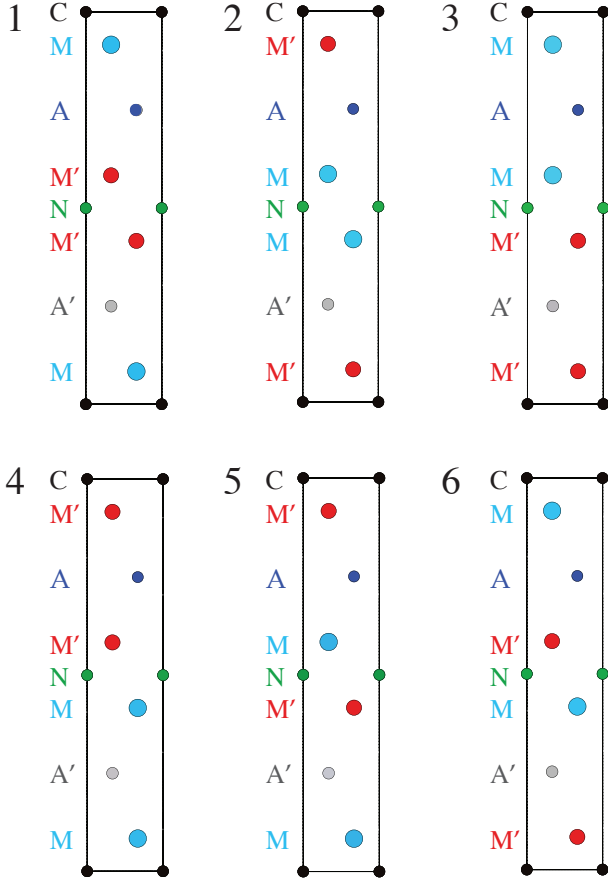
FIG. 2. (color online) Structure models for the six unique configurations of an $(MM^{'})_2(AA^{'})(CN)$ compound. In configurations 1 and 2, M layers envelop C and N layers, respectively. In configurations 3 and 4, they envelop A and $A^{'}$ layers, respectively. In configurations 5 and 6, M layers alternate with $M^{'}$ layers.

III. RESULTS AND DISCUSSION

A. Most Stable M_2AX Configurations

To reduce the number of possible configurations that need to be considered, we first identify empirical rules for the most favorable configuration of all compositions in the 8-atom unit cell and then investigate the effect of in-plane mixing on the energy.

For all 10,530 M_2AX compositions we consider 8-atom unit cells with the characteristic $P6_3/mmc$ hexagonal M_2AX phase crystal structure and cell volumes adjusted based on the covalent radii of atoms in the cell. Even for these simple ordered cells, there are several possible atomic configurations for compositions that contain more than one M and A element. Specifically, there are 3 unique ways to arrange the atoms for the $(MM^{'})_2AX$ composition, 4 unique arrangements for $(MM^{'})_2(AA^{'})X$ and $(MM^{'})_2A(XX^{'})$, and 6 unique arrangements for $(MM^{'})_2(AA^{'})(XX^{'})$. Optimizing the structures of each
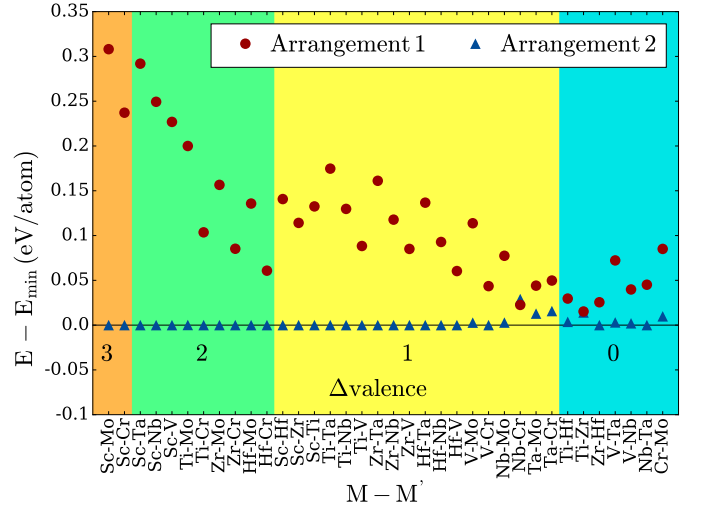

FIG. 3. (color online) Relative stability of configurations 1 and 2 from Figure 2 for 36 $(MM^{'})_2(AlAs)(CN)$ compositions. The x-axis is arranged from left to right in order of decreasing valence difference between M and $M^{'}$ to show that the preference between configurations 1 and 2 is most marked when the valence difference is large, indicated by the colored regions. All energies are shown relative to the most stable of all 6 configurations, so a positive value of $E - E_{min}$ for both configurations indicates that one of configurations 3-6 is the most stable. These cases are rare, and in all other cases the energies of configurations 3-6 are all between those of configurations 1 and 2.

of these arrangements would increase the number of calculations from 10,530 to 37,455. To avoid this additional expense without sacrificing accuracy, we identify empirical rules for the most favorable arrangement based on the energy of the 6 possible arrangements shown in Figure 2 for the subset of 36 $(MM^{'})_2(AlGa)(CN)$ and 36 $(MM^{'})_2(AlAs)(CN)$ compositions with M, M' = Sc, Ti, V, Cr, Zr, Nb, Mo, Hf, and Ta.

We find that when the A elements are Al and Ga, either configuration 1 or 2 from Figure 2 is always the most favorable. For the more dissimilar A elements Al and As, Figure 3 shows the energy of configuration 1 and 2 relative to the lowest energy configuration. We observe that the same trend mostly holds and that the energy difference decreases with the difference in the valences and atomic radii of the two M elements. Moreover, we observe that when the M elements are from different groups in the periodic table, the M element of higher valence preferentially bonds to C. When the M elements are from the same group, the one with the larger atomic radius preferentially bonds to C.

The large energy differences between configurations 1 and 2, particularly for the cases with large difference in valence, suggests that the creation of maximally ionic M-X bonds is the most important driving factor in determining the optimal configuration, and that the choice of configuration significantly affects the stability of M_2AX
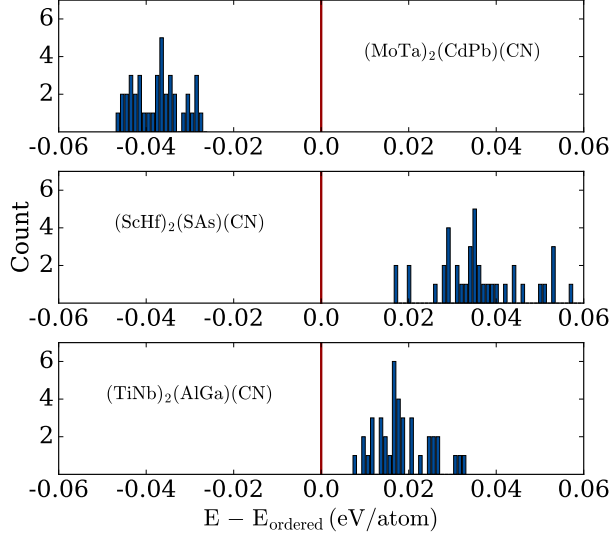
FIG. 4. Energy per atom of the ordered 8 atom cells (red lines) in relation to the distribution of energies calculated for 40 configurations with random in- plane mixing of the corresponding 32 atom cells (blue histograms). The greatest enthalpy of mixing is observed for $(MoTa)_2(CdPb)(CN)$, at 47 meV/atom.

FIG. 5. Calculated formation energies for the 49 experimentally known M_2AX phases. Negative (stable) or small positive (slightly unstable) formation energies are predicted for all 49 compounds, with Hf_2SnN showing the highest metastability of 26 meV/atom.

phases with multiple M and X elements. These predictions are in agreement with previous calculations, which identify M-X bonds as being responsible for close to 50% of the total bond order in M_2AX phases.[33]

Based on our empirical observations, we assume configuration 2 for all combinations of M elements is the lowest energy configuration. Based on the energy differences shown in Figure 3, we estimate a maximum error of less than 30 meV/atom for every combination of M elements. The M element in that configuration is selected as the one of higher valence or with larger atomic radius, if the valences are the same.

To investigate the effect of in-plane mixing on the energy, we create larger $2\times2\times1$ cells containing 32 atoms for three $(MM')_2(AA')(CN)$ compounds. Figure 4 compares the energy of 40 random configurations of M/M', A/A', and C/N atoms on their respective sites for these three compounds. We find that for two of the compounds, the ordered 8 atom cell is energetically favored over in-plane mixing, while for the third, $(MoTa)_2(CdPb)(CN)$, the in-plane mixing is favored but still within 50 meV/atom of the energy of the ordered 8 atom cell. This value is sufficiently small, such that the ordered 8-atom cell provides a reasonably accurate energy estimate even for cases with in-plane mixing.

To estimate the gain in Gibbs free energy at finite temperature due to in-plane mixing, we apply the regular solution model. This model assumes the ideal entropy of mixing, which provides an upper bound for the configurational entropy. The ideal entropy of mixing per formula unit (f.u.) for the M_2AX phases is
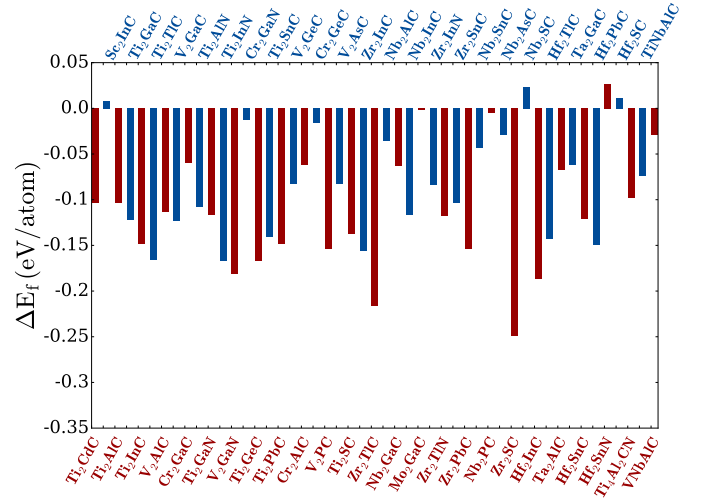
$$\Delta S^{mix} = -k_B \left[2\ln\left(\frac{1}{n_m}\right) + \ln\left(\frac{1}{n_a}\right) + \ln\left(\frac{1}{n_x}\right) \right],$$

where n_m, n_a, and n_x are the number of M, A, and X elements (either 1 or 2) in a given composition. For the $(MM')_2(AA')(CN)$ composition, where n_m, n_a, and n_x are each equal to 2, the entropy of mixing is 0.24 meV/f.u.·K, or 0.06 meV/atom·K. The energies for in-plane mixing of the $(TiNb)_2(AlGa)(CN)$ and $(ScHf)_2(SAs)(CN)$ compounds shown in Figure 4 are about 20 and 40 meV/atom, respectively, resulting in critical temperature for complete in-plane mixing of 330 and 670 K, respectively. We expect that many of the $(MM')_2(AA')(CN)$ systems exhibit similar energies of mixing and in-plane disorder at high temperature.

While calculating the enthalpy of in-plane mixing for all M_2AX phases is outside of the current scope, it is an important consideration for future detailed work on selected compositions.

B. M_2AX Phase Stability

Next, we determine the stability of the 10,530 possible M_2AX compositions relative to the competing phases in each system. The structures of the competing phases are obtained from the Materials Project database[37] and optimized using the parameters as described in Sec. II.

Before asserting its predictive capability, we benchmark the screening method against the experimentally known stable compounds. As mentioned above, 49 M_2AX phases have successfully been synthesized, provid-

ing the screening with a substantial benchmarking sample size. Figure 5 shows the formation energies of all 49 experimentally stable M_2AX phases with respect to the most stable competing phases. Eleven of the 49 experimentally stable phases were already reported in the Materials Project database. We predict negative (stable) formation energies for 45 of the 49 stable M_2AX phases, with the remaining four (Sc_2InC, Nb_2SC, Hf_2SnN, and Hf_2SC) possessing small positive (unstable) formation energies of 8, 23, 26, and 11 meV/atom, respectively.

The slightly positive formation energies for four of the 49 experimentally observed MAX phases indicate that either entropic contributions such as the configurational entropy discussed earlier are important for the stabilization of these compounds or that the choice of exchange-correlation functional affects these energy differences. Slightly positive DFT formation energies are common across experimentally phases; in fact, nearly 20% of the compounds in the Inorganic Crystal Structure Database[51] have instabilities above 36 meV/atom.[52] To ensure that we do not overlook a viable M_2AX compound, we select a 30 meV/atom cutoff for the formation energies in our study. We furthermore note that even compounds above this cutoff could be stabilzed by their configurational entropy of mixing.

We identify 3,140 of the 10,530 M_2AX compositions with formation energies below 30 meV/atom, highlighting the large potential size of this family. Of these 3,140 compositions, 301 have formation energies below -100 meV/atom. 27 of these 301 are among the compositions that have already been synthesized. 134 of the 301 contain Ti, 112 contain In, and 261 contain C; these are the elements that are present the largest number of M_2AX compounds for M, A, and X, respectively. All 3,140 stable M_2AX compounds can be found in the MaterialsWeb online database at `http://materialsweb.org`. The MaterialsWeb database provides the relaxed structures and stability information for all investigated M_2AX compounds.

The four most stable M_2AX phases that were previously unknown are $Ti_2V_2Ga_2CN$, $Sc_2Zr_2Ga_2CN$, $Zr_2Hf_2Ga_2CN$, and $Zr_2Mo_2Ga_2CN$. All four have $A =$ Ga and $X =$ C-N, and M is always a mixture of two metals. This means that mixtures are among the most stable of all M_2AX phases, and that the solid-solution space should certainly be explored in searches for stable M_3AX_2 and M_4AX_3 phases.

The automatic data-mining approach for the identification of the most stable competing phases minimizes the number of false positives in our study of the M_2AX phase stability. A previous study[30] that relied on manual selection, identified the same competing phases for Sc_2AlC, Mo_2GeC, and Ti_2AsC. However, for Ta_2GeC, our datamining approach identifies competing phases with a combined enthalpy that is 0.3 eV/atom lower than the manually selected ones. This illustrates the power of databases and high-throughput approaches and the importance of exhaustive searches for competing phases. On the other
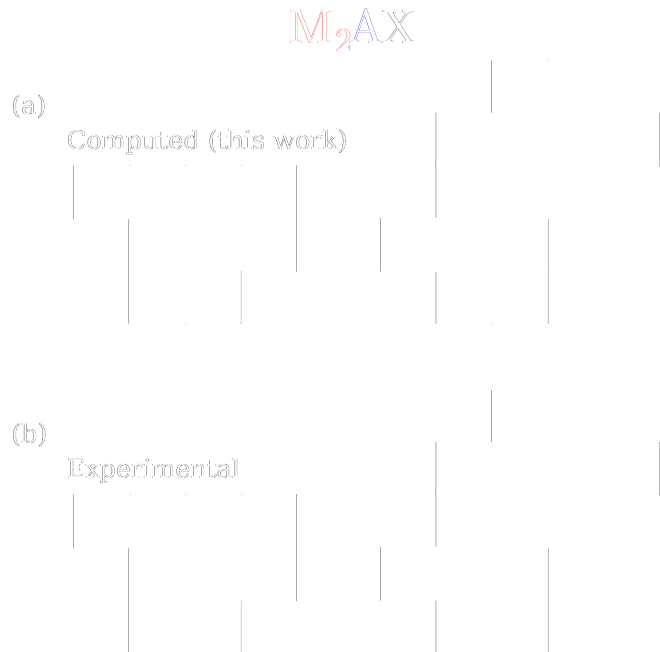

FIG. 6. Frequency of elements occurring in stable M_2AX phases, that are (a) computationally predicted in this work, and (b) experimentally synthesized. In (a), the number of compositions with formation energies < -100 meV/atom that contain a given element is given for all M, A, and X elements. In (b), the number of synthesized M_2AX phases containing the element is given. Similar trends are found.

hand, for V_2AlC, the manually selected phases are lower in energy by 0.045 eV/atom, since they included the hypothetical V_3AlC_2 phase, which has not been synthesized and does not currently exist in the Materials Project database.

C. Trends of Phase Stability

Several trends emerge from the calculated stability of the 10,530 M_2AX compositions. The first one is illustrated in Figure 6, which compares the distribution of compositions for the predicted highly stable ($\Delta E_F < -100$ meV/atom) and experimentally synthesized M_2AX phases. In both cases, M_2AX phases that contain $M =$ Ti, $A =$ group 13 elements, and $X =$ C present the largest group of stable M_2AX phases. Overall, we find a close agreement in the frequency of occurence for each element in the predicted and experimentally synthesized M_2AX phases. Our screening indicates that the dearth of experimental Si-, P-, Ge- and As-containing M_2AX phases is likely due to lack of thermodynamic stability of these phases and not due to kinetics. Previously, a similar thermodynamic argument explained the relatively small number of only 13 stable $M_{n+1}AX_n$ phases with $n = 2, 3$.[16]

For the unstable M_2AX phases, we find that the stable

competing phases, or decomposition products, are generally binary M-X compounds with either elemental A and M or M-A compounds forming from the excess A and M. Experimentally, most M_2AX phases decompose to highly defective M-X compounds, *e.g.* $TiC_{0.67}$, with elemental A diffusing between the layers at high temperatures.[53]

We predict considerably higher relative numbers of stable Sc- and Cd-based M_2AX phases than have been created experimentally. This is an interesting result for several reasons. First, it could mean that a large number of Sc- and Cd-containing M_2AX phases are stable and their synthesis has simply not yet been attempted. Alternatively, it could indicate that there are more stable competing phases for Sc- and Cd- containing M_2AX phases than the ones presently found in the Materials Project database. If this is the case, careful analysis of the decomposition products after attempted synthesis for these M_2AX phases could lead to the discovery of new compounds, or at least to the addition of new compounds to the Materials Project database. Finally, it could be the result of some more complex phenomena governing the stability of these compounds, which are outside the scope of our screening approach. For example, the effect of oxygen incorporation, which is known to occur in MAX phases,[54–58] is not considered in our models but could affect the stability of some M_2AX compounds.

To uncover which properties of the compounds contribute most strongly to their formation energies, we perform a principal component analysis (PCA) on a dataset comprising all formation energies and descriptors associated with each elemental component. The descriptors (atomic radius, ionic radius, valence electron count, first ionization potential and electronegativity) were defined as both the difference of the elements on a site and as the average of the descriptors on a site, in order to reduce the bias in the subsequent analysis. PCA operates by defining a linear combination of the descriptors that captures the most independent information in the dataset.[59–61] In this way, by ordering the new axes in terms of the corresponding information, the data may be described in fewer dimensions with a minimum loss of information. The relationships uncovered and the corresponding visualizations become more robust and interpretable.

We determine the correlation of the formation energy with the descriptors using the loading values, which define the transformed axis system. The correlation is defined based on the relative positioning of each descriptor relative to the formation energy within this transformed space. We center the data at the origin prior to the analysis, so that the correlation between two data points is proportional to the cosine of the angle formed between the points and the origin. Alternatively, the correlation between the formation energy and the descriptors may be defined as

$$\text{Importance of } k^{\text{th}} \text{ variable} = \frac{p_1^k p_1^t + p_2^k p_2^t}{\sum\limits_r (p_1^r p_1^t + p_2^r p_2^t)} \times 100,$$

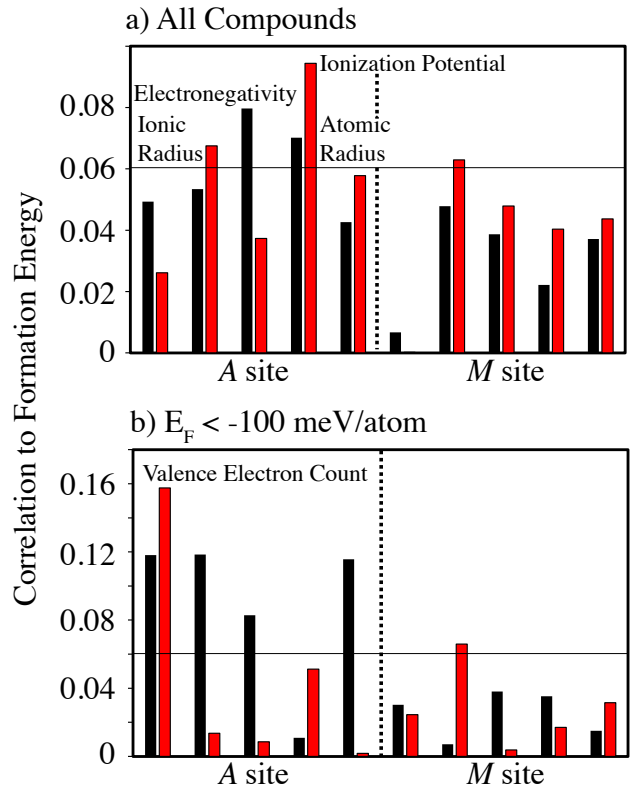where p are the loadings values, k refers to the descrip-

FIG. 7. Identifying the descriptors correlated with formation energy, and the difference in the corresponding physics when considering the entire chemical space (a) versus only those with low formation energy (b). The black (left) bars represent descriptors which are calculated as average value of the descriptor for all elements on that site, while the red (right) bars represent descriptors which are calculated as the difference for the elements. The A site has larger impact on the formation energy, particularly for low formation energy compounds.

tors, and t is the target, *i.e.* the formation energy. This equation is used to obtain the data in Figure 7. While this equation is shown for two components, we include five components in our analysis, which capture 84.7% of the variance of the entire data. This compression from 30 to 5 dimensions allows us to identify which descriptors most impact the formation energy.

Figure 7 shows the relationships between the descriptors and the formation energy obtained from the PCA for the M and A sites. We find no significant correlations for the X sites. The PCA identifies five descriptors, which most impact the formation energy, with the A site having slightly larger impact for compounds with low formation energy, and the M site having a significant impact for the overall search space.

An important question is whether the chemical correlations differ for compounds with low and high formation energies. This is critical if we want to define design rules with the intent of identifying stable M_2AX phases.
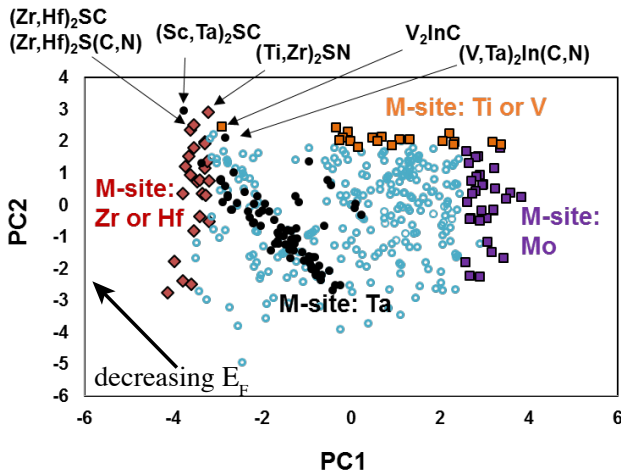
FIG. 8. Mapping of the compounds in the principal component (PC) space. The clustering of chemistries (black circles representing compounds containing Ta, red diamonds representing Zr and/or Hf, purple squares representing Mo, and orange squares representing Ti and/or V) captures relationships between formation energy (target direction) and chemistry.

Indeed, we find that there is a difference between the analysis including all compounds shown in Fig. 7(a) versus that for compounds whose formation energies are less than -100 meV/atom shown in Fig. 7(b).

In the case of assessing all compounds, we find that the primary parameters of interest are the average electronegativity, difference in ionic radius, and difference in ionization potential for the A site elements, and differences in ionic radius for the M site elements. When the analysis was repeated for low formation energy compounds, a different set of critical descriptors emerges. These included the difference in valence electron count, the average ionic radius, and the average atomic radius for A site, and the difference in ionic radius for M site elements. This captures the difference in physics and provides design guidelines and future inputs into defining quantitative regression models for predicting virtual compounds. A multiple linear regression between formation energy and the five identified descriptors results in an R^2 correlation of 71.6%, demonstrating that these descriptors capture the physics defining formation energy for these compounds.

We also use PCA to develop a mapping of the compounds, with the mapping based on PCA score values, which define the compounds in the new axis space in Figure 8. In this case, we focus on the two most critical axes (principal components PC_1 and PC_2). This mapping shows clustering with the chemistries defined on the descriptor base used. We observe that the formation energy becomes more negative along the decreasing PC_1 and increasing PC_2 directions. From this, we identify the M site elements most corresponding with the target direction are Ti and V, while some Ta, Zr and Hf-

containing compounds also meet the criteria, as shown in the labeled compounds. Many of the compounds furthest from the target region contain Mo on the M-site. These findings are consistent with Figure 6, which projects Ti, Zr, Hf, V and Ta as among the six most common elements in M_2AX phases with low formation energies, while Mo was among the least common. Also, when looking at the labeled compounds, In or S occupy the A site, again agreeing with Figure 6.

D. Properties of Predicted M_2AX Phases

Compositions with useful properties can now be isolated from among those predicted to be stable. For example, any magnetic compositions are of interest for potential application in writeable storage devices with good toughness.

Of the 3,140 stable M_2AX phases, two exhibit magnetic moments greater than 1 μ_B/M atom in our initial screening, which assumes a ferromagnetic ordering. These compounds are Cr_2InN and Cr_4CdInN_2 with formation energies of 7 and 21 meV/atom. Calculations show that the energy of Cr_4CdInN_2 cannot be significantly lowered by mixing Cd and In in-plane. To determine the most stable magnetic ordering, we calculate the energies of two antiferromagnetic configurations for these two M_2AX phases, in addition to the ferromagnetic and nonmagnetic configurations already considered.

We find that the lowest-energy configuration is indeed ferromagnetically ordered. This is in contrast to the Cr-based M_2AX phases that have already been synthesized, which have previously been predicted to order antiferromagnetically (Cr_2AlC, Cr_2GaC, and Cr_2GeC).[62–65]

The ferromagnetic Cr_2InN and Cr_4CdInN_2 phases display magnetic moments of 1.18 and 1.08 μ_B, respectively. These magnetic moments are similar to that of metallic Ni, indicating that both materials could be used commercially in machinable and corrosion resistant magnetic components if they display reasonable Curie temperatures. To provide a first estimate of the order of magnitude of the Curie temperature of Cr_2InN and Cr_4CdInN_2, we compare their magnetization energy to that of of five related transition metal compounds, YNi_3, MnAs, MnSb, MnBi, and CrO_2. The magnetization energy is the energy difference between the ferromagnetic and nonmagnetic state and calculated using the same convergence parameters as for the MAX phases.

Figure 9 shows that the experimental Curie temperatures,[66–68] T_c, correlate reasonably well with the magnetization energies for the five related transition metal compounds, YNi_3, MnAs, MnSb, MnBi, and CrO_2. This indicates that the magnetization energy can be used as a computationally efficient estimator for the Curie temperature.

The magnetization energies of Cr_2InN and Cr_4CdInN_2 are very similar with 34 and 35 meV/atom. The observed correlation between magnetization energy and Curie tem-
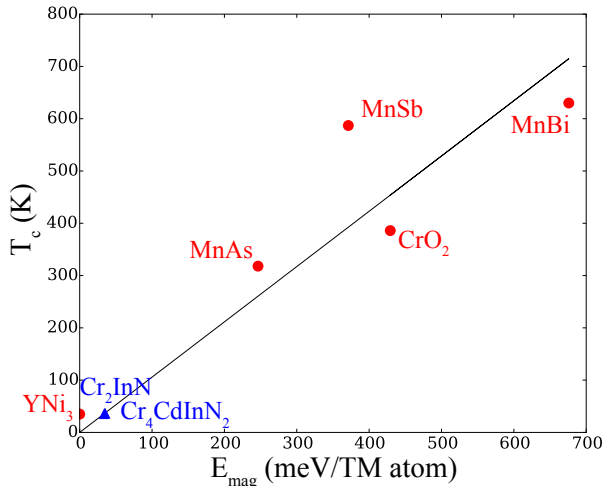
FIG. 9. The Curie temperatures of YNi_3, MnAs, MnSb, MnBi, and CrO_2 vs. their magnetization energies per transition metal atom, as calculated using the inputs in our framework. The correlation indicates that higher magnetization energies generally lead to higher Curie temperatures. The best fit line is forced to intercept the origin, and is used to project the Curie temperatures of Cr_2InN and Cr_4CdInN_2.

perature illustrated in Fig. 9 indicates that both materials have a Curie temperature of the order of 50K. This suggests that if the synthesis conditions overcome the slightly positive formation energies, that both Cr_2InN and Cr_4CdInN_2 are the most promising low-temperature ferromagnets among the 10,530 M_2AX phases considered.

IV. CONCLUSIONS

Using a high-throughput framework coupled to density-functional theory, we calculated the formation energies of the 10,530 M_2AX compositions with the goal to identify thermodynamically stable compositions and aid experimental synthesis efforts. We characterized the crystal structures of solid solution M_2AX phases and narrowed the number of promising M_2AX phases from 10,530 to 3,140. Furthermore, 301 compositions have been identified that should be readily synthesizable, with formation energies below -100 meV/atom relative to their competing phases. Among the 3,140 predicted stable compounds, we find two, Cr_2InN and Cr_4CdInN_2, that show promise as ferromagnets. We observe general trends in the stability data, such as that choosing A elements of similar radii and M elements of similar valence and electronegativity enhances the thermodynamic stability of solid-solution M_2AX phases. All the data generated in this high-throughput screening is available in the database provided at `https://materialsweb.org`.

The results of this systematic search for stable M_2AX phases demonstrate the power of leveraging large-scale computational efforts to discover new compounds, and indicate there is still plenty of room for discovery in this already large family of compounds. We have demonstrated the ability of computational techniques to screen compounds for stability against bulk phases in a framework that can easily be applied to other classes of compounds, including the more elusive $n > 1$ $M_{n+1}AX_n$ phases.

[1] R. Armiento, B. Kozinsky, M. Fornari, and G. Ceder, Physical Review B **84**, 014103 (2011).

[2] R. Armiento, B. Kozinsky, G. Hautier, M. Fornari, and G. Ceder, Physical Review B **89**, 134103 (2014).

[3] G. Ceder, Y.-M. Chiang, D. Sadoway, M. Aydinol, Y.-I. Jang, and B. Huang, Nature **392**, 694 (1998).

[4] C. Toher, J. J. Plata, O. Levy, M. de Jong, M. Asta, M. B. Nardelli, and S. Curtarolo, Physical Review B **90**, 174107 (2014).

[5] P. Eklund, M. Beckers, U. Jansson, H. Högberg, and L. Hultman, Thin Solid Films **518**, 1851 (2010).

[6] M. W. Barsoum, MAX *phases: properties of machinable ternary carbides and nitrides* (John Wiley & Sons, 2013).

[7] I. Salama, T. El-Raghy, and M. Barsoum, Journal of Alloys and Compounds **347**, 271 (2002).

[8] H. Zhang, Y. Zhou, Y. Bao, M. Li, and J. Wang, Journal of the European Ceramic Society **26**, 2373 (2006).

[9] M. Barsoum, T. El-Raghy, and M. Ali, Metallurgical and Materials Transactions A **31**, 1857 (2000).

[10] M. W. Barsoum, Progress in Solid State Chemistry **28**, 201 (2000).

[11] H. Nowotny, P. Rogl, and J. C. Schuster, Journal of Solid State Chemistry **44**, 126 (1982).

[12] J. Schuster, H. Nowotny, and C. Vaccaro, Journal of Solid State Chemistry **32**, 213 (1980).

[13] S. Gupta and M. Barsoum, Journal of The Electrochemical Society **151**, D24 (2004).

[14] X. Xu, T. L. Ngai, and Y. Li, Ceramics International **41**, 7626 (2015).

[15] A. Petruhins, A. S. Ingason, J. Lu, F. Magnus, S. Olafsson, and J. Rosen, Journal of Materials Science **50**, 4495 (2014).

[16] A. Mockutė, (2014).

[17] Q. Wang, A. F. Renteria, O. Schroeter, R. Mykhaylonka, C. Leyens, W. Garkas, and M. to Baben, Surface and

[18] Coatings Technology **204**, 2343 (2010).

[18] S. Myhra, J. Summers, and E. Kisi, Materials Letters **39**, 6 (1999).

[19] A. Crossley, E. H. Kisi, J. B. Summers, and S. Myhra, Journal of Physics D: Applied Physics **32**, 632 (1999).

[20] M. Radovic and M. W. Barsoum, American Ceramics Society Bulletin **92**, 20 (2013).

[21] B. Pécz, L. Tóth, M. di Forte-Poisson, and J. Vacas, Applied Surface Science **206**, 8 (2003).

[22] J.-C. Nappé, P. Grosseau, F. Audubert, B. Guilhot, M. Beauvy, M. Benabdesselam, and I. Monnet, Journal of Nuclear Materials **385**, 304 (2009).

[23] F. Meng, L. Chaffron, and Y. Zhou, Journal of Nuclear Materials **386**, 647 (2009).

[24] M. Naguib, M. Kurtoglu, V. Presser, J. Lu, J. Niu, M. Heon, L. Hultman, Y. Gogotsi, and M. W. Barsoum, Advanced Materials **23**, 4248 (2011).

[25] M. Naguib, O. Mashtalir, J. Carle, V. Presser, J. Lu, L. Hultman, Y. Gogotsi, and M. W. Barsoum, ACS Nano **6**, 1322 (2012).

[26] M. Ashton, K. Mathew, R. G. Hennig, and S. B. Sinnott, The Journal of Physical Chemistry C **120**, 3550 (2016).

[27] M. Naguib, J. Come, B. Dyatkin, V. Presser, P.-L. Taberna, P. Simon, M. W. Barsoum, and Y. Gogotsi, Electrochemistry Communications **16**, 61 (2012).

[28] M. Naguib, J. Halim, J. Lu, K. M. Cook, L. Hultman, Y. Gogotsi, and M. W. Barsoum, Journal of the American Chemical Society **135**, 15966 (2013).

[29] M. Ashton, R. G. Hennig, and S. B. Sinnott, Applied Physics Letters **108**, 023901 (2016).

[30] M. Dahlqvist, B. Alling, and J. Rosén, Physical Review B **81**, 220102 (2010).

[31] J.-P. Palmquist, S. Li, P. Å. Persson, J. Emmerlich, O. Wilhelmsson, H. Högberg, M. Katsnelson, B. Johansson, R. Ahuja, O. Eriksson, *et al.*, Physical Review B **70**, 165401 (2004).

[32] V. Keast, S. Harris, and D. Smith, Physical Review B **80** (2009).

[33] S. Aryal, R. Sakidja, M. W. Barsoum, and W.-Y. Ching, Physica Status Solidi (b) **251**, 1480 (2014).

[34] F. Meng, Y. Zhou, and J. Wang, Scripta Materialia **53**, 1369 (2005).

[35] J. Wang and Y. Zhou, Journal of Physics: Condensed Matter **16**, 2819 (2004).

[36] Y. Zhou, F. Meng, and J. Zhang, Journal of the American Ceramic Society **91**, 1357 (2008).

[37] A. Jain, S. P. Ong, G. Hautier, W. Chen, W. D. Richards, S. Dacek, S. Cholia, D. Gunter, D. Skinner, G. Ceder, and K. A. Persson, APL Materials **1**, 011002 (2013).

[38] G. Kresse and J. Hafner, Physical Review B **47**, 558 (1993).

[39] G. Kresse and J. Furthmüller, Physical Review B **54**, 169 (1996).

[40] P. E. Blöchl, Physical Review B **50**, 17953 (1994).

[41] G. Kresse and D. Joubert, Physical Review B **59**, 1758 (1999).

[42] J. P. Perdew, K. Burke, and M. Ernzerhof, Physical Review Letters **77**, 3865 (1996).

[43] A. Jain, G. Hautier, C. J. Moore, S. P. Ong, C. C. Fischer, T. Mueller, K. A. Persson, and G. Ceder, Computational Materials Science **50**, 2295 (2011).

[44] S. F. Sousa, P. A. Fernandes, and M. J. Ramos, The Journal of Physical Chemistry A **111**, 10439 (2007).

[45] A. D. Becke, The Journal of Chemical Physics **97**, 9173 (1992).

[46] S. Kurth, J. P. Perdew, and P. Blaha, International Journal of Quantum Chemistry **75**, 889 (1999).

[47] D. C. Langreth and M. Mehl, Physical Review B **28**, 1809 (1983).

[48] M. Fishman, H. L. Zhuang, K. Mathew, W. Dirschka, and R. G. Hennig, Physical Review B **87**, 245402 (2013).

[49] A. Jain, S. P. Ong, G. Hautier, W. Chen, W. D. Richards, S. Dacek, S. Cholia, D. Gunter, D. Skinner, G. Ceder, and K. a. Persson, APL Materials **1**, 011002 (2013).

[50] S. P. Ong, S. Cholia, A. Jain, M. Brafman, D. Gunter, G. Ceder, and K. A. Persson, Computational Materials Science **97**, 209 (2015).

[51] G. Bergerhoff, R. Hundt, R. Sievers, and I. Brown, Journal of Chemical Information and Computer Sciences **23**, 66 (1983).

[52] Y. Wu, P. Lazic, G. Hautier, K. Persson, and G. Ceder, Energy & Environmental Science **6**, 157 (2013).

[53] J. Emmerlich, D. Music, P. Eklund, O. Wilhelmsson, U. Jansson, J. M. Schneider, H. Högberg, and L. Hultman, Acta Materialia **55**, 1479 (2007).

[54] J. Rosen, P. Persson, M. Ionescu, A. Kondyurin, D. McKenzie, M. Bilek, *et al.*, Applied Physics Letters **92**, 4102 (2008).

[55] T. Liao, J. Wang, M. Li, and Y. Zhou, Journal of Materials Research **24**, 3190 (2009).

[56] M. Dahlqvist, B. Alling, I. A. Abrikosov, and J. Rosén, Physical Review B **81**, 024111 (2010).

[57] P. Å. Persson, J. Rosén, D. McKenzie, and M. Bilek, Physical Review B **80**, 092102 (2009).

[58] M. Baben, L. Shang, J. Emmerlich, and J. M. Schneider, Acta Materialia **60**, 4810 (2012).

[59] S. R. Broderick, A. Bryden, S. K. Suram, and K. Rajan, Ultramicroscopy **132**, 121 (2013).

[60] S. R. Broderick, H. Aourag, and K. Rajan, Journal of the American Ceramic Society **94**, 2974 (2011).

[61] A. N. Andriotis, G. Mpourmpakis, S. Broderick, K. Rajan, S. Datta, M. Sunkara, and M. Menon, The Journal of chemical physics **140**, 094705 (2014).

[62] M. Dahlqvist, B. Alling, and J. Rosén, (2014).

[63] A. Petruhins, A. S. Ingason, M. Dahlqvist, A. Mockute, M. Junaid, J. Birch, J. Lu, L. Hultman, P. O. Persson, and J. Rosen, Physica Status Solidi (RRL)-Rapid Research Letters **7**, 971 (2013).

[64] M. Mattesini and M. Magnuson, Journal of Physics: Condensed Matter **25**, 035601 (2012).

[65] W. Zhou, L. Liu, and P. Wu, Journal of Applied Physics **106**, 3501 (2009).

[66] C. Kittel, *Introduction to solid state physics* (Wiley, 2005).

[67] K. Buschow and R. Van Essen, Solid State Communications **32**, 1241 (1979).

[68] I. Dubenko, R. Levitin, A. Markosyan, A. Petropavlovsky, and V. Snegirev, Journal of Magnetism and Magnetic Materials **90**, 715 (1990).